

Ultralow-Power Electronics for Cardiac Monitoring

Lorenzo Turicchia, Bruno Do Valle, *Student Member, IEEE*, Jose L. Bohorquez, *Member, IEEE*, William R. Sanchez, Vinith Misra, Leon Fay, Maziar Tavakoli, and Rahul Sarpeshkar, *Senior Member, IEEE*

Abstract—Ultralow-power electronics for cardiac monitoring make possible the development of new light-weight and low-cost devices that are ideal for long-term medical measurements and home-based tele-monitoring services. Nowadays, these devices are seen as a critical technology for reducing health-care costs. In this paper, we present several methods for reducing power consumption while retaining the precision necessary for cardiac monitoring. In particular, we describe a micropower electrocardiograph, an ultralow-power pulse oximeter, an ultralow-power phonocardiograph, an integrated-circuit switched-capacitor model of the heart, and an ultracompact and efficient lithium-ion battery charger. These components are, to our knowledge, currently the most power-efficient or minimal-size designs present in the literature in each respective category.

Index Terms—Battery charger, blood oxygen saturation, cardiac monitoring, electrocardiograph (EKG), heart model, low power, medical instrumentation, phonocardiograph (PCG), photo-plethysmogram (PPG), pulse oximeter, wearable monitoring.

I. INTRODUCTION

HYPERTENSION is the most prevalent treatable cause of vascular events [1]. On the other hand, according to the National Center for Health Statistics, 29% of adult Americans have hypertension and an additional 28% have prehypertension [2]. Recently, there have been questions about the common practice of measuring only the mean blood pressure when assessing the vascular risk factor [1]. In fact, the variability of the blood pressure, thought to be random by clinicians, seems to have an

important role in the progression of organ damage and in the triggering of vascular events. A similar situation seems to exist for the mean heart rate versus heart-rate variability (HRV). The HRV, in fact, has been proven to carry important information complementary to the mean heart value. It can be used as a predictor of risk after acute myocardial infarction and as an early warning sign of diabetic neuropathy [3]. Consequentially, the possibilities offered by convenient new low-cost devices to constantly monitor the cardiovascular system and to gather data are now extremely clinically important.

In addition, heart-disease management plays a major role among health-care policies due to the high cost of treating this disease. According to the American Heart Association, heart-failure patient care cost \$24 billion in the United States in 2003, with hospitalization accounting for 70% of this expense [4]. As pointed out by the Home-Care Management Systems study (TEN-HMS), cost reduction can be achieved using home-based tele-monitoring services for heart-failure patients [4]. This cost saving is primarily due to the fact that home tele-monitoring patients spend fewer days in the hospital than normal patients. In addition, home tele-monitoring has led to very high patient satisfaction [4]. Therefore, there is considerable interest in finding heart-monitoring devices that can be comfortably used by patients at home. In the past, such devices were only used for measurements not achievable in a hospital (e.g., long-term monitoring). Nowadays, these devices are seen as critical for reducing skyrocketing health-care costs.

Research on electronics for wearable medical monitoring has focused on reducing the overall power consumption of such devices. Power consumption is the most critical limitation since such instruments need batteries to be light and wearable and/or require a long time between battery recharges. The cost of the battery is also a key limiting factor for the widespread adoption of such devices. Energy-harvesting battery-free medical-monitoring devices also have severe power constraints [5]. In this paper, we summarize some innovations developed by our group toward heart-monitoring devices that are free from the weight, cost, and recharging needs of big batteries. To achieve this goal, we developed three kinds of components: 1) ultralow-power sensor circuits able to transduce and amplify the medical signal of interest; 2) an integrated-circuit model of the medical system from which we want to infer relevant properties; and 3) an ultracompact and efficient lithium-ion battery charger. The goal of this paper is to review these innovations, thereby offering a vision of how ultralow-power operation can be achieved for cardiac-monitoring applications. The detailed design of ultralow-power electronics for implantable and noninvasive applications in a broad range of medical contexts may be found in [5].

A previous version of this paper, with a focus on wearable and battery-free operation via RF energy-harvesting antennas and a

Manuscript received March 29, 2010; revised June 24, 2010; accepted July 20, 2010. Date of publication September 23, 2010; date of current version October 01, 2010. This paper was recommended by Associate Editor S. Mirabbasi.

L. Turicchia, B. Do Valle, W. R. Sanchez, and R. Sarpeshkar are with the Department of Electrical Engineering and Computer Science, Massachusetts Institute of Technology, Cambridge, MA 02139 USA (e-mail: turic@mit.edu; brunogr@mit.edu; wasan79@mit.edu; rahuls@mit.edu).

J. L. Bohorquez was with the Department of Electrical Engineering and Computer Science, Massachusetts Institute of Technology, Cambridge, MA 02139 USA. He is now with Convergence Medical Devices, Winchester, MA 01890 USA (e-mail: bohorquez@cmdevices.com).

V. Misra was with the Department of Electrical Engineering and Computer Science, Massachusetts Institute of Technology, Cambridge, MA 02139 USA. He is now with the Department of Electrical Engineering, Stanford University, Stanford, CA 94305 USA (e-mail: vinith@stanford.edu).

L. Fay was with the Department of Electrical Engineering and Computer Science, Massachusetts Institute of Technology, Cambridge, MA 02139 USA. He is now with SRI International, Menlo Park, CA 94025 (e-mail: leon.fay@gmail.com).

M. Tavakoli was with the Department of Electrical Engineering and Computer Science, Massachusetts Institute of Technology, Cambridge, MA 02139 USA. He is now with Linear Technology Corp., North Chelmsford, MA 01863 USA (e-mail: mtavakoli@linear.com).

Color versions of one or more of the figures in this paper are available online at <http://ieeexplore.ieee.org>.

Digital Object Identifier 10.1109/TCSI.2010.2071610

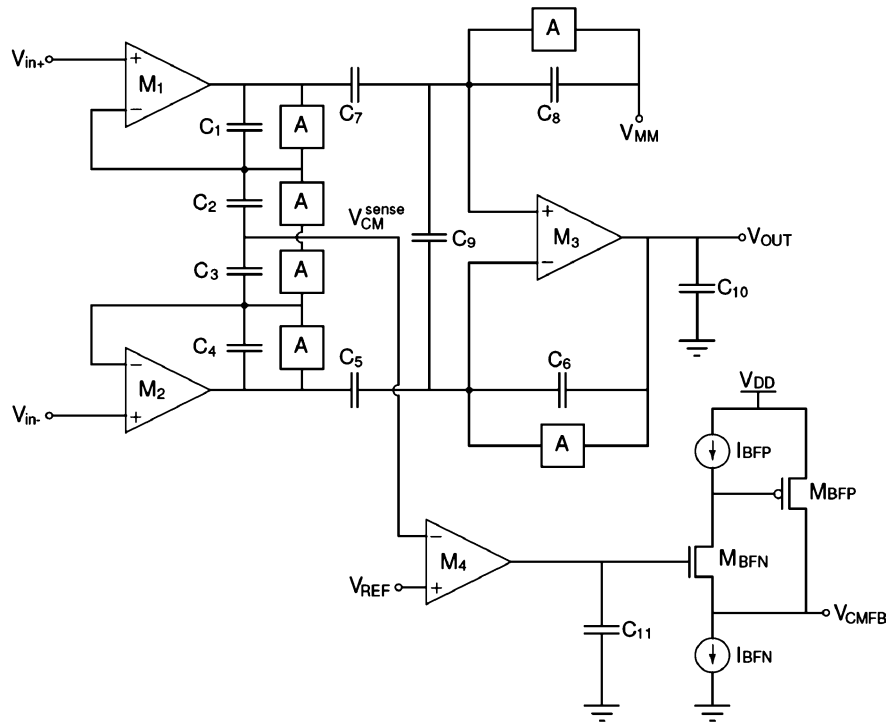


Fig. 1. Electrocardiogram amplifier schematic.

micropower event-monitor chip has been presented at a conference [6]. In this invited journal paper, we expand on some of the circuits in the conference paper that are useful in implantable applications and also present new circuits for battery recharging.

The paper is organized as follows: In Sections II, III, and IV, we describe the design of a micropower electrocardiograph, an ultralow-power pulse oximeter, and an ultralow-power phonocardiograph, respectively. In Section V, we present an integrated-circuit switched-capacitor model and implementation of the heart. In Section VI we describe the design of a novel, ultracompact lithium-ion battery-charging circuit intended for operation in a wirelessly rechargeable medical device. In Section VII, we conclude by summarizing our contributions.

II. A MICROPOWER ELECTROCARDIOGRAPH

The electrocardiogram (EKG or ECG)—the recording of the electrical activity of the heart over time—is one of the fundamental components in a medical-monitoring setup because it allows important diagnostic analysis of the heart's functionality. In its simplest circuit implementation, the EKG amplifier is a high-input-impedance differential amplifier with high common-mode rejection ratio (CMRR) and $\sim\mu\text{V}$ input-referred noise—needed because the high-impedance input nodes pick up a great amount of interfering common-mode 60 Hz signal and because P-waves in EKG signals are faint. The design of such amplifiers with a micropower budget and without stringent matching requirements can be difficult.

Fig. 1 shows our micropower EKG amplifier schematic. It is based on a standard two-gain-stage instrumentation-amplifier topology. The high input impedance of this topology compensates for the impedance of the electrode connections. Furthermore, a common-mode feedback path is introduced to create an “active ground” that suppresses 60 Hz noise [7] and eliminates

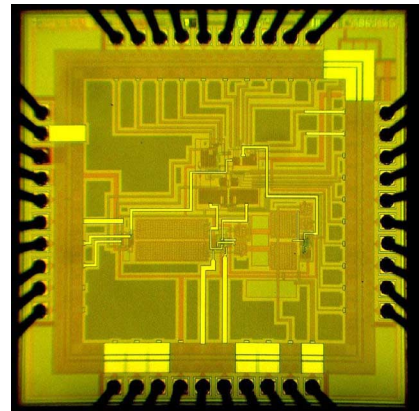


Fig. 2. Micropower EKG die micrograph (1 mm²).

the extremely stringent matching requirements of purely feed-forward designs. This is facilitated by the instrumentation-amplifier topology, which extracts the input common-mode signal in addition to amplifying the differential signal.

The input nodes V_{in+} and V_{in-} are connected to the input electrodes, the common-mode feedback output V_{CMFNB} is connected to the active-ground electrode, and V_{OUT} is the amplifier output. The amplifiers M_1 , M_2 , M_3 , and M_4 are 5-transistor pFET-differential-pair operational transconductance amplifiers (OTAs). The first-stage amplifier (M_1 , M_2) uses a 1.5 V supply while M_3 and M_4 operate at 3 V. The dual-supply requirement can be accommodated via series connection of two batteries or by using intermediate outputs in rectenna-based charge-pumps in energy-harvesting systems [6], [8].

The amplifier was fabricated in an AMI 0.5 μm process (Fig. 2) and has a total power consumption of 2.76 μW , 8.1 μV_{rms} input-referred noise, 45.3 dB gain, 290 Hz bandwidth, 41.8 dB dynamic range, and CMRR (at 60 Hz) of 90 dB

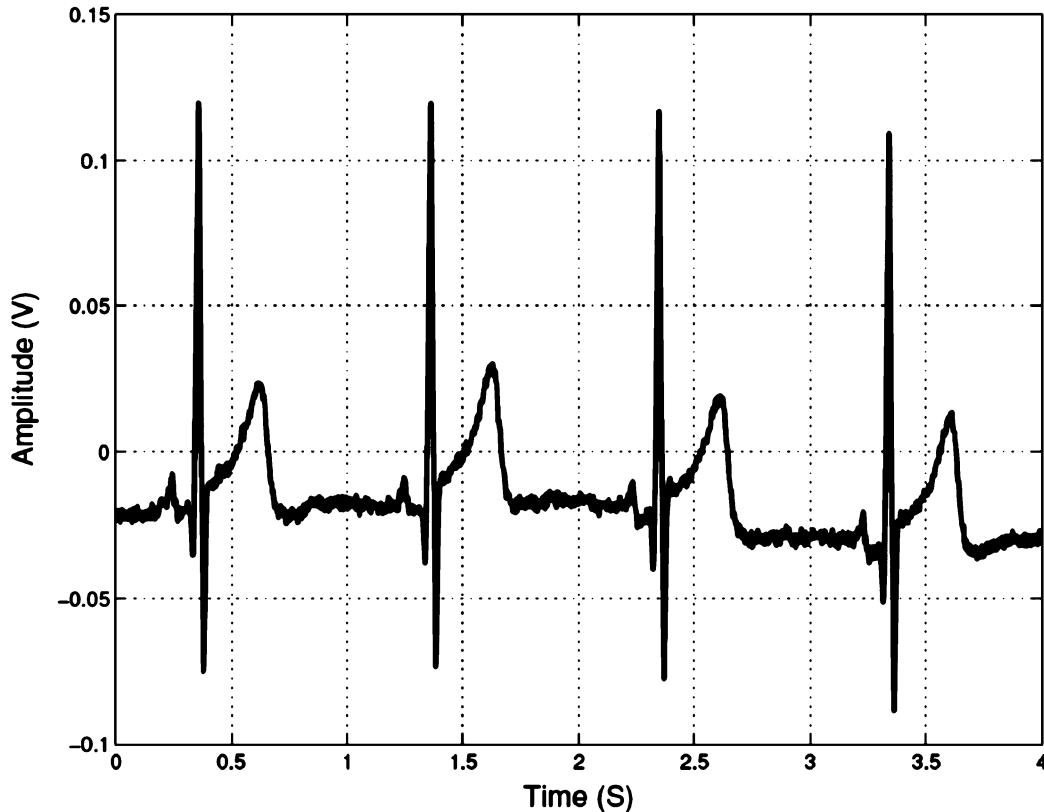


Fig. 3. An example EKG signal captured with the amplifier from a subject with a healthy heart.

[8]. These specifications make it, to our knowledge, the lowest power actively grounded EKG amplifier built thus far. Other actively grounded EKG amplifier designs consume $20 \mu\text{W}$ or more [9]. Purely feed-forward strategies without active grounding require high differential matching and are relatively costly.

Our power reduction is due to eight design choices: 1) the usage of subthreshold transistor operation to improve noise efficiency; 2) the usage of active grounding with common-mode feedback (CMFB) [7]; 3) the usage of gain-setting capacitors in parallel with “adaptive elements” (shown as the “A” blocks in Fig. 1 and functioning as back-to-back diodes) instead of resistors [10]; 4) the usage of half-rail supply operation wherever possible (the half-rail supply saves power when extra headroom is unnecessary while full-rail supply increases dynamic range at the output and helps accommodate the input common-mode operating range); 5) the optimization of the power allocations among amplifier blocks; 6) the optimization of the sizing of devices to improve matching and reduce noise; 7) the usage of pFET input devices for all amplifiers to minimize $1/f$ noise; and 8) the usage of a super source-follower (SSF) [11], revealed by the transistor-and-current-source circuit of Fig. 1, for obtaining low output impedance, which is useful in quenching 60 Hz interference signals.

The significant power reduction achieved by our design does not come at the cost of measurement quality. Fig. 3 shows EKG measurements obtained from a healthy subject using FS-TB1 hydrogel electrodes from Skintact attached to a leg and both arms, and connected to the corresponding terminals of the EKG amplifier. One may observe that the captured EKG waveform

has good signal-to-noise ratio (SNR) and that the “P” waves are clearly observable.

III. AN ULTRALOW-POWER PULSE OXIMETER

Pulse oximetry is a method for monitoring the oxygen saturation (S_pO_2) of a patient’s hemoglobin molecules. Oxygen saturation provides a comprehensive measurement of the patient’s cardio-respiratory health status. Pulse oximeters measure variations in the optical density of transmission in the arteries due to their contraction and relaxation as a function of time. A pulse-oximeter output waveform is known as a photo-plethysmogram, or PPG. Pulse-oximeter measurements involve the creation of intense flashes of light that make PPG recording very expensive in terms of power consumption and consequently impractical for wearable patient monitoring.

We addressed this expensive power budget by developing an ultralow-power pulse oximeter that achieves more than an order-of-magnitude reduction in power consumption over the best commercial pulse oximeters. This power reduction is due to the creation of a novel logarithmic transimpedance amplifier that eliminates the need for bright LED light. Our design is based on the standard logarithmic transimpedance photoreceptor [10] with the addition of three major improvements: 1) the gain of the amplifier in the photoreceptor is distributed over many stages to increase its gain-bandwidth product for a given power consumption; 2) the addition of an adaptive loop-gain mechanism to automatically adjust loop gain based on the light intensity, obtaining less speedup for high light levels (to prevent potential instability) and more speedup for low light levels (to achieve larger bandwidth); and 3) the usage of a common-

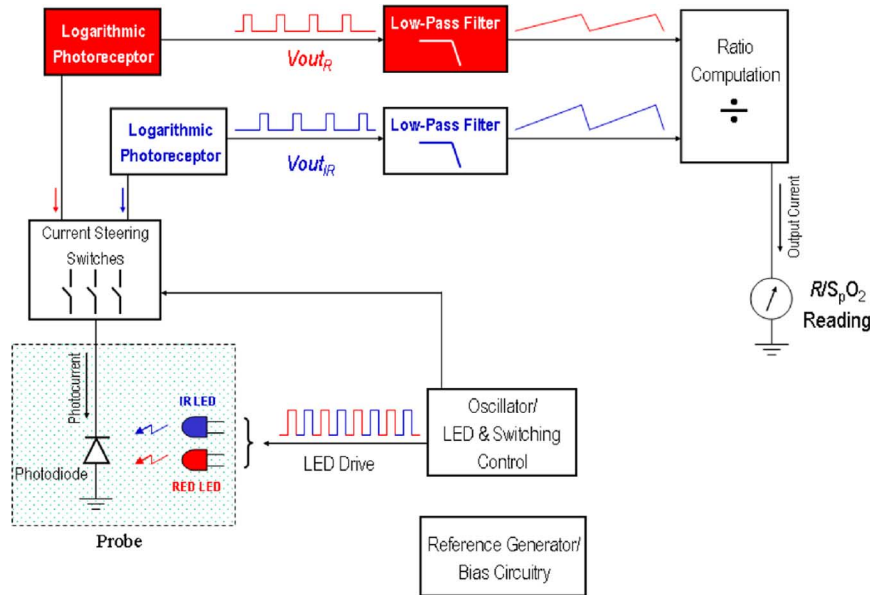


Fig. 4. The architecture of our low-power pulse oximeter.

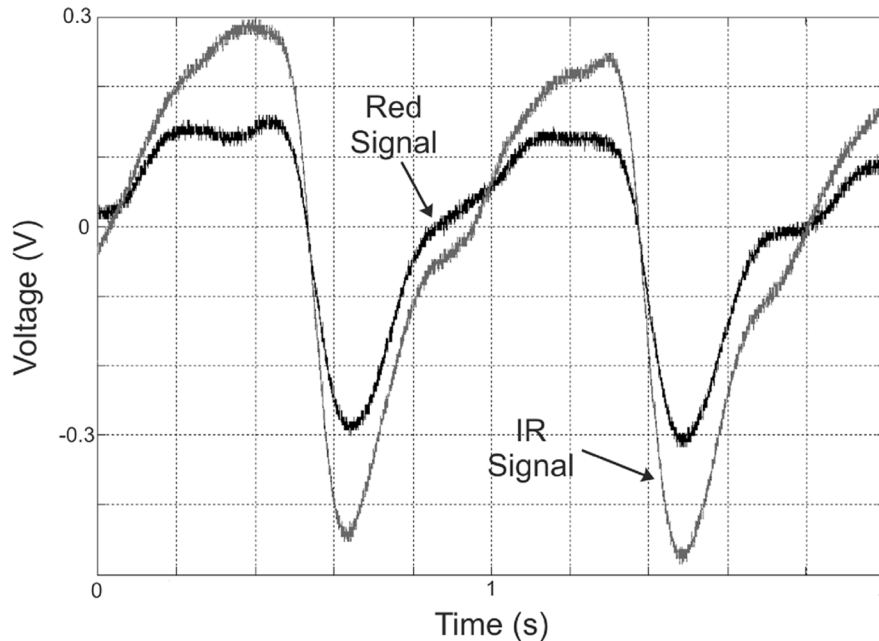


Fig. 5. Pulse-oximeter waveforms captured from a healthy subject.

gate stage for sensing the input photocurrent and converting it to a logarithm, exploiting the method of unilateralization for speeding up feedback-amplifier response [12].

Fig. 4 shows a block diagram of our pulse oximeter system. The input to the chip is a photocurrent coming from a probe connected to the patient and the output of the chip is a current directly proportional to measured oxygen saturation of the patient's hemoglobin molecules. The light needed in the pulse oximeter is provided by two LEDs with red and infrared light. The LEDs are driven by a square wave with a small duty cycle. Both LEDs are alternatively illuminated and the photocurrent generated by a single photodiode is split, switched, and steered into two different paths, one channel sensitive to the red light and the other to IR light. The signals are then amplified by our novel transimpedance amplifiers, low-pass filtered, and divided.

Details on the signal processing needed to obtain oxygen saturation from the measured photodiode current can be found in [12].

Fig. 5 shows PPG measurements obtained by our pulse oximeter using, as the sensing element, a commercial finger clip transmittance reusable probe manufactured by Nonin Medical, Inc. (model 8000AA), and connected to an healthy subject. We also statistically analyzed the differences between the oxygen saturation readings from our pulse oximeter and a reference oximeter for 11 subjects. Our measured accuracy was -1.2% mean and 1.5% standard deviation, which are higher than commonly required in medical practice.

Our pulse oximeter was fabricated in an AMI $1.5\ \mu\text{m}$ process (Fig. 6) and has a total power consumption of $4.8\ \text{mW}$. State-of-the-art commercial implementations dissipate nearly $55\ \text{mW}$.

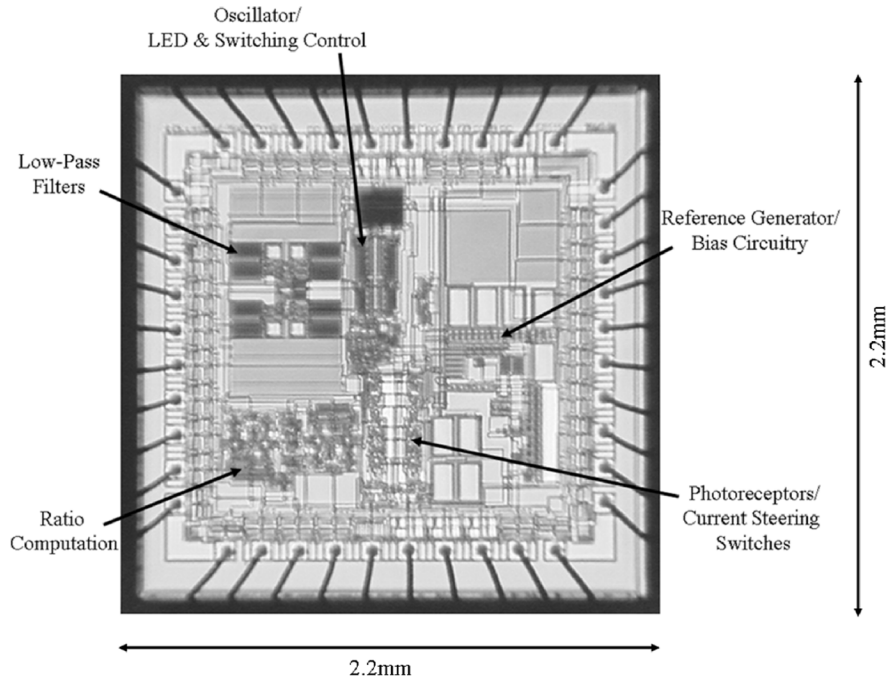


Fig. 6. Die micrograph of our pulse oximeter chip with its building blocks marked.

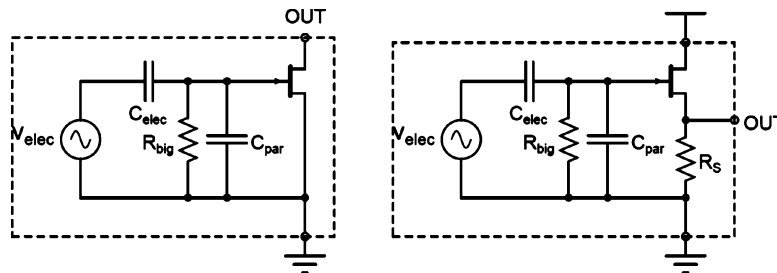


Fig. 7. Circuit diagram of common electret microphones, two-terminal (left) and three-terminal (right).

Our pulse oximeter also performs its entire signal processing in the analog domain, obviating the need for an A-to-D and DSP and leads to a very area-efficient single-chip system. Simple extensions to our adaptive energy-efficient transimpedance amplifier can lead to submilliwatt power consumption without compromising performance [12].

IV. AN ULTRALOW-POWER PHONOCARDIOGRAPH

Phonocardiography (PCG) is the recording of the sounds produced by the heart over time. This method, although diagnostically poor compared with more modern heart analysis techniques, has very important advantages such as being low-cost, low-power, maintenance-free, robust to 60 Hz pickup, and requiring no electrical contact with the body.

Microphones can be used to monitor heart sounds. Commercial electret microphones contain built-in low-noise JFETs for buffering. Two configurations, as shown in Fig. 7, are commonly used. In two-terminal microphones, shown on the left, the drain of the n-type JFET, which is normally a depletion-mode device, acts as the output terminal. It is usually connected to an external resistive load, creating a common-source amplifier. The gate voltage is internally tied to ground at DC with the large resistor R_{big} , while C_{par} is a small, unwanted parasitic capacitance. The

incoming sound pressure wave creates the voltage source v_{elec} in series with the electret capacitance C_{elec} . Three-terminal microphones, shown on the right, configure the JFET as a source follower, and are typically more expensive.

Here, we use a two-terminal microphone (Panasonic omnidirectional electret condenser microphone WM-63PR), but replace the resistive load with a programmable current source running off a very low supply voltage to save power. In this regime, the JFET is unsaturated and acts as a voltage-controlled resistor. In this configuration, we can monitor the cardiovascular system with an inexpensive device and at the same time use very little power [13].

Measured waveforms are shown in Fig. 8 using a bias current of $30 \mu\text{A}$ and power-supply voltage of 0.5 V. We have simultaneously measured the sound produced by the blood at the wrist and at the neck of a healthy subject. The bottom part of the picture is the thresholded version of the sound recorded by the microphone. The waveform at the wrist is delayed relative to that at the neck by about 95 ms because of the time taken by the systolic pulse to propagate down the length of the arm. This delay can be used to provide information about blood pressure [15]. The continuous monitoring of the blood pressure enabled by this strategy is orders-of-magnitude cheaper in power than a

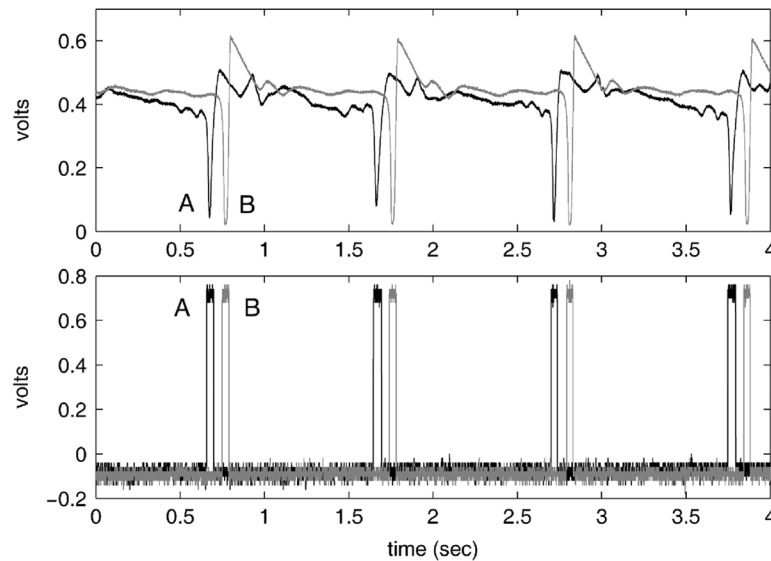


Fig. 8. PCG waveforms measured at neck and wrist. The top figure shows the PPG while the bottom figure shows thresholded events generated from the PPG.

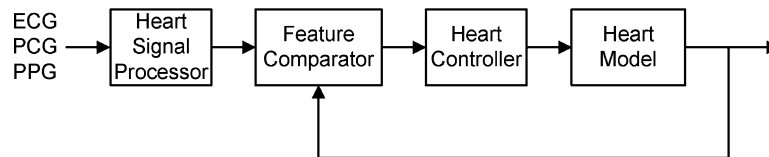


Fig. 9. Concept of a “heart locked loop (HLL).”

classic method that uses a sphygmomanometer, but calibration techniques are required to get absolute pressure [16].

V. AN INTEGRATED-CIRCUIT MODEL OF THE HEART

In addition to the power savings that can be achieved by careful design of analog subsystems, novel signal-processing techniques can be employed to drastically reduce the total power consumption of a medical-monitoring device. System tradeoffs must be employed to minimize the total system power, which may include adding signal processing on the wearable device (with its associated power cost) that may drastically reduce the amount of information that has to be transmitted. Since data transmission is often power intensive, extracting the salient features from collected raw data is often preferable to transferring the raw data itself. Here we describe a new approach to extracting the most critical physiological features by using an analysis-by-synthesis technique, which potentially requires very little power to operate.

Fig. 9 shows an analysis-by-synthesis block diagram that creates what we term a “heart locked loop” (HLL) in analogy with phase locked loops (PLL) used in other communication systems. The feature comparator, heart controller, and heart model in the HLL are respectively analogous to the phase detector, loop filter, and voltage-controlled oscillator (VCO) in a PLL. In a PLL, feedback is used to lock the frequency and phase of a VCO to those of an input signal. The output of the loop filter in a PLL is the precise tuning voltage required at the input of the VCO to match its frequency to that of the input signal. If the information of interest was the input signal’s frequency, and the relationship between the tuning voltage and VCO frequency was known precisely, only the tuning voltage data would have to be transmitted.

This is clearly far more energy efficient than transmitting the entire input signal, and would result in energy savings.

The HLL in Fig. 9 is similar. The heart signal processor transforms ECG, PCG, and PPG information to cardiac waveforms that can be compared to those from a heart model via the feature comparator. Errors produced by the comparator are processed by the heart-controller block to update the heart model in a feedback fashion such that it is consistent with the observed data. Eventually, the HLL locks the heart model output to the input heart signal, and the heart controller’s output yields the optimal cardiovascular parameters of interest (just as the loop filter’s output would yield the tuning voltage of interest). The amount of data required to transmit these parameters could potentially be far less than transmitting the ECG, PCG, and PPG signals themselves, resulting in significant power savings.

Combining the HLL with low-power sensors allows the transmission of highly significant cardiovascular parameters, thus saving transmission power. For further energy savings, parameter thresholds can be stored in the system and information can be transferred only when some cardiovascular characteristics are not considered normal.

To build an energy-efficient HLL, a low-power model of the heart is needed. We have derived an electronic model of the heart using an analogy between mechanical and electronic systems such that: pressure is analogous to voltage, fluid volume velocity is analogous to current, and fluid volume is analogous to charge [17]. Compliance, inertance, and mechanical damping are then analogous to capacitance, inductance, and electrical resistance. Fig. 10 shows our simplified model of the heart where typical mechanical parameters are converted to electrical parameters. The transmission line comprising resistors, inductors, and ca-

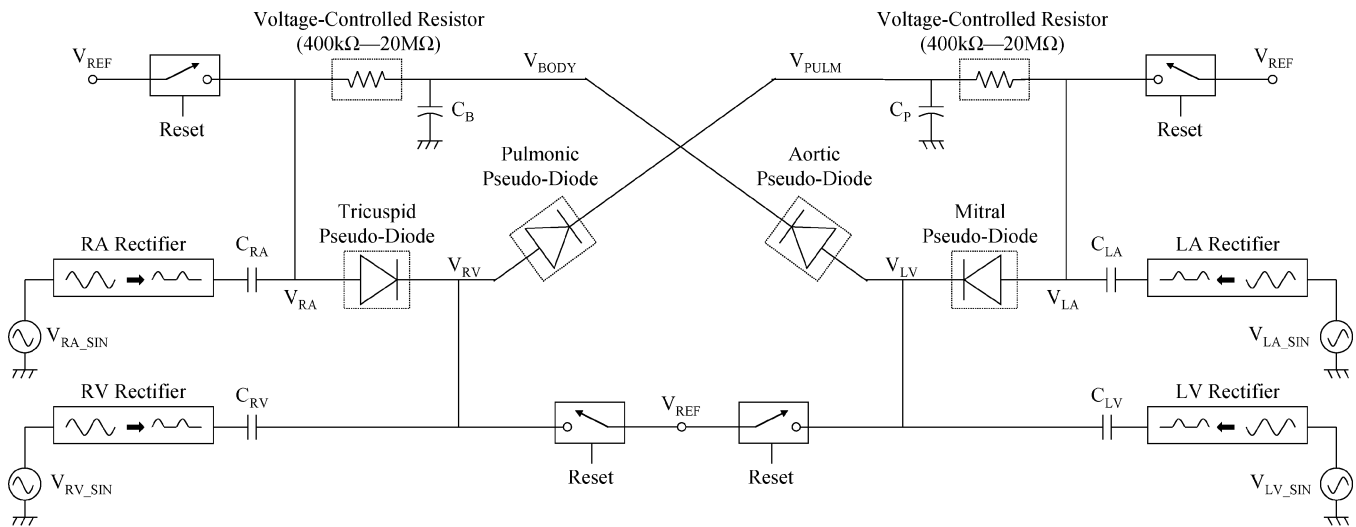


Fig. 10. System schematic for model of the human heart.

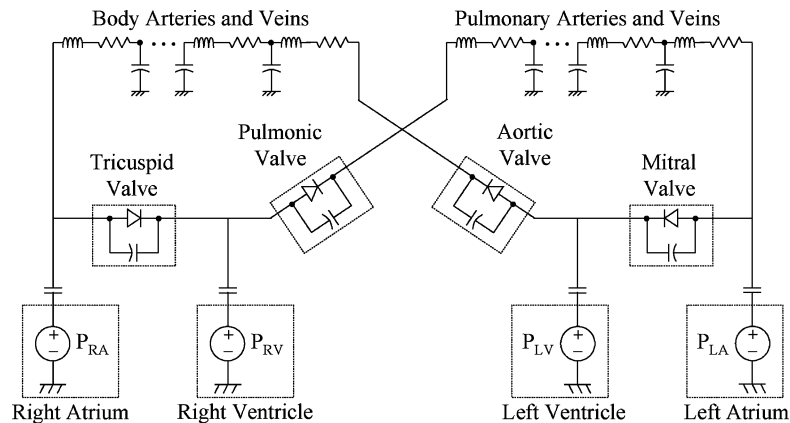


Fig. 11. Simplified electrical model of the human heart.

capacitors represents the distributed impedance of the circulatory system. The four valves in the heart are modeled as ideal diodes in parallel with capacitors.

The model of Fig. 10 was further simplified to the extremely simple one in Fig. 11 [17]. The inductances are not included here, since good accuracy in a heart model is obtained without their use [14]. We have also introduced some reset switches that are not part of the heart model itself, but are used to create an initial condition in the system that allows all of the components to function properly. The value V_{REF} in Fig. 11 corresponds to the average pressure in the cardiovascular system plus an arbitrary offset used so that all components operate within their acceptable common-mode voltage range.

We have developed three ultralow-power circuits that are equivalent to the basic component types that make up our simplified heart model: pseudodiodes (zero-threshold diodes), rectifiers, and large current-controlled resistors [17]. Fig. 12 shows the pseudodiode circuit used to model heart valves. Fig. 12(b) shows a functional diagram of the circuit comprising a comparator and a CMOS transmission-gate switch. If the voltage on the “anode” (labeled A) is greater than that on the “cathode” (labeled C), the comparator output turns the CMOS switch on allowing current to flow from A to C. This is analogous to a heart valve opening and allowing blood flow when

the pressure potential across it is positive. If current begins to flow from C to A through R_{ON} , however, the resulting negative voltage across the comparator’s input causes the switch to turn off. This is analogous to a heart valve closing to prevent blood from flowing in the wrong direction. The benefit of using this circuit instead of an actual diode is that the voltage potential required to initiate current flow is practically zero. This improves the fidelity of the electrical model to the mechanical nature of the heart; particularly in low supply-voltage systems.

Fig. 13 shows the current-controlled large-resistor circuit (CCLR). The circuit is composed of two back-to-back operational transconductance amplifiers (OTA) which individually output a current equal to the voltage across them divided by their transconductance G_m . Two OTAs were used to model the bidirectional current flow of a resistance. Source degeneration is used to increase the linear range of the OTA and reduces slewing due to fast input changes. The circuit thus implements an effective resistance of value $1/G_m$ which is variable and set by the control current I_{TUNE} .

A chip implementing these circuits was fabricated in an AMI $0.5 \mu\text{m}$ process. Although this chip implements a simplified model of the heart, it reproduces important features of heart function. Fig. 14 shows measured voltage waveforms for the left side of the heart and equivalent pressure values. The most im-

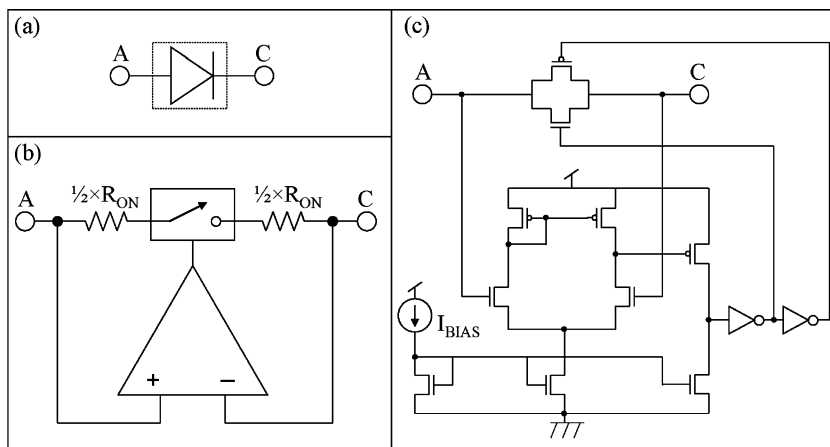


Fig. 12. Pseudodiode circuit: (a) symbol; (b) functional diagram; and (c) schematic. The pseudodiode circuit functions like a diode with zero-volt threshold; positive voltage (forward bias) closes a switch and allows flow, while negative voltage (reverse bias) opens a switch and limits flow.

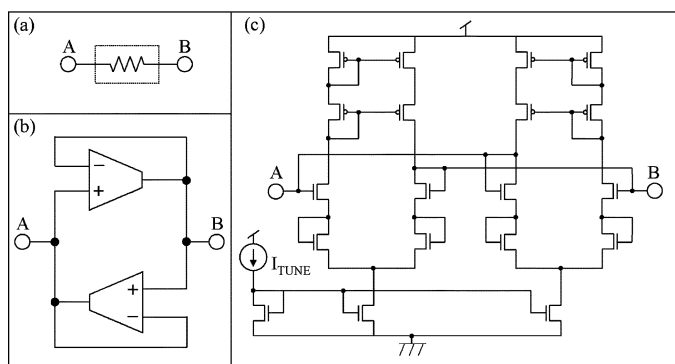


Fig. 13. Current-controlled large resistor circuit: (a) symbol; (b) functional diagram; and (c) schematic. The effective resistance is inversely proportional to I_{TUNE} .

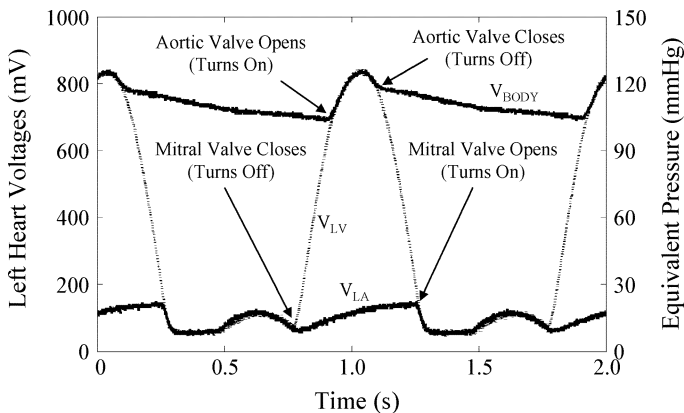


Fig. 14. Measured voltage waveforms for the left half of the heart and equivalent pressure values.

portant features present in the real cardiac cycle are simulated by the chip.

VI. AN ULTRACOMPACT LITHIUM-ION BATTERY CHARGING CIRCUIT

In this section, we present a novel, ultracompact lithium-ion (Li-ion) battery-charging circuit intended for operation in a wirelessly rechargeable medical device. Li-ion batteries are a popular choice due to their ability to provide relatively high performance in both energy and power densities, of ~ 158 Wh/Kg and ~ 1300 W/Kg, in geometries practical for

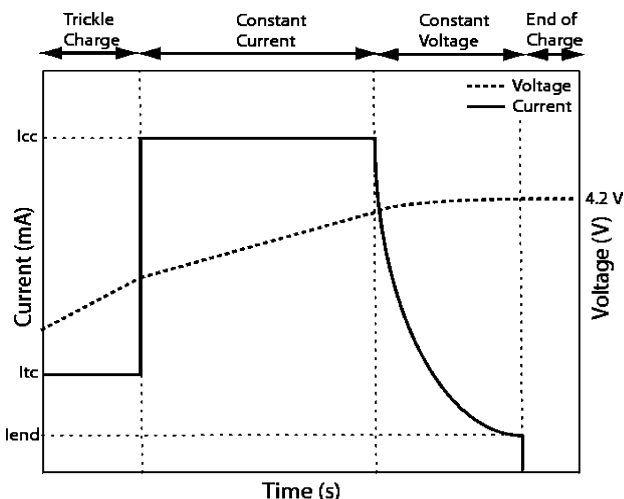


Fig. 15. Theoretical Li-ion charging profile.

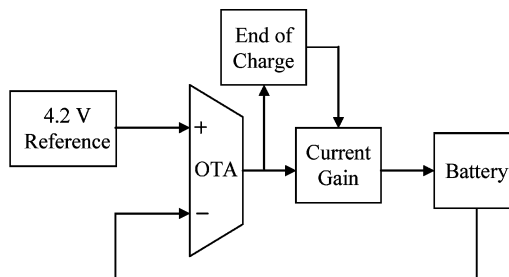


Fig. 16. Simplified battery charger block diagram.

medical devices [18]. The charger presented here takes advantage of the tanh output current profile of a subthreshold operational transconductance amplifier (OTA) to automatically and smoothly transition between constant-current and constant-voltage charging regimes. Additional area-consuming and power-consuming complex control circuitry, typically implemented in a digital controller, thus become unnecessary.

The charging profile of a Li-ion battery can be divided into four distinct regions as illustrated by Fig. 15: trickle-charge, constant-current, constant-voltage, and end-of-charge. Trickle charging is required only if the battery is deeply discharged (voltage is less than 3 V). During trickle-charge, the battery is charged with a small amount of current, typically no more than

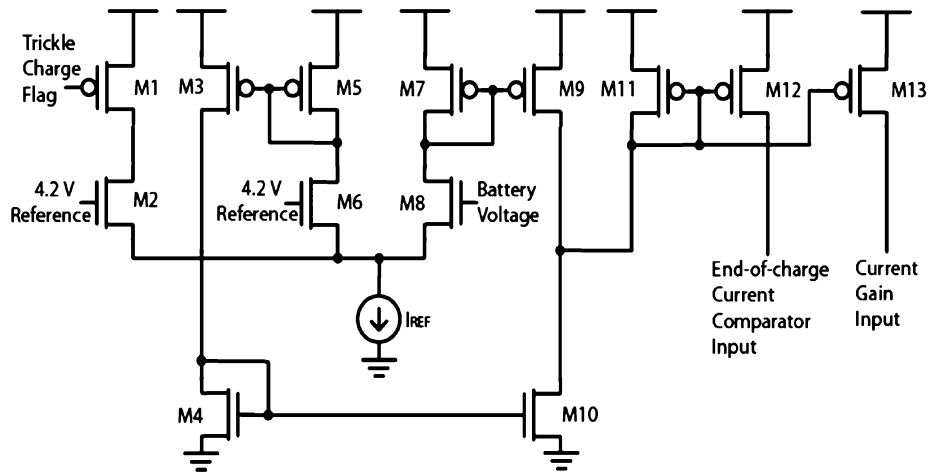


Fig. 17. OTA and trickle-charge circuit schematic.

0.1 times the rated capacity of the battery [19]. Above 3.0 V, the battery may be charged at higher currents; this is the constant-current region. As the battery voltage approaches 4.2 V, the charging profile enters the constant-voltage region. In this region, the charging current should be progressively decreased as the battery voltage approaches 4.2 V. Charging current should be decreased until a certain threshold is met, which is usually about 2% of the rated battery capacity [19]. Once this charging current is reached, the charger enters the end-of-charge region.

A simplified block diagram of our circuit topology is illustrated in Fig. 16. The circuit consists of four major blocks: a 4.2 V reference, an OTA, a current gain stage, and an end-of-charge detector. The output of the bandgap is approximately 1.2 V, so in order to get the 4.2 V reference, we included a noninverting op-amp with a gain of 3.5. The reference must be very precise since undercharging a Li-ion battery by 1.2% of the 4.2 V target value can result in a 9% reduction in capacity [19]. To get an error less than 1% in the 4.2 V reference, we included 7 bits of digital trimming so that we can compensate for process variation, transistor mismatch, and fluctuations in the power-supply voltage of the bandgap circuit, which may be obtained via energy harvesting from a wireless source [5], [6].

The OTA compares the battery voltage to the 4.2 V reference in order to determine the charging current. The OTA is designed in the subthreshold regime in order to save power and also to reduce its linear range, which is close to 100 mV. So, for battery voltages less than approximately 4.1 V, the OTA's output is saturated and the battery is charged with maximum current (constant-current regime). As the battery voltage reaches 4.1 V, the OTA enters its linear regime and the output current begins to decrease (constant-voltage regime). The end-of-charge is detected by comparing the output of the OTA to a reference current. When the battery gets close to 4.2 V and the output of the OTA is less than the end-of-charge reference current, the charging is terminated.

To implement the trickle-charge portion of the battery profile, a standard OTA topology is modified to that shown in Fig. 17 with the primary modification being the addition of the transistors M1 and M2. If the battery voltage is less than 3 V, the *Trickle Charge Flag* is low enabling M1. In this case, transistor M2 conducts some current, which reduces the OTA's output via

current stealing of its bias current. The reduction in charging current during trickle-charge is proportional to the ratio of the W/L of M2 to the W/L of M6 or M8. Once the battery voltage crosses the 3 V threshold, the *Trickle Charge Flag* goes high disabling the current path through M1 and M2. As a result, the current output of the OTA is increased to its maximum value.

The current-gain stage is composed of current mirrors that increase the current output of the OTA from a few hundred nano-amps to whatever current is required to charge the battery. Since this charging current is only dependent on the current-gain stage, the overall control scheme is useful in both low-power and high-power battery-charging applications.

Fig. 18 shows the measured results of a battery-management chip that exploits the circuit of Fig. 17 to charge a 25 mAh test battery. In this experiment we set V_{DD} to 5 V. The output of the bandgap is approximately 1.2 V, so in order to get a 4.2 V reference, we included a noninverting op-amp with a gain of 3.5. During constant-current operation, the circuit charges the battery with approximately 2 mA. The constant-voltage region begins when the battery reaches approximately 4.1 V. The transition between constant-current and constant voltage is smooth since our control loop is based on a simple tanh function. According to Fig. 18, the charging current decreases as the battery voltage goes from 4.1 V to 4.2 V, reaching the end of charge when the current is approximately 0.26 mA. At the end of charging, the battery voltage is 4.21 V, providing an accuracy of 99.8%. The relatively long charging time in our implementation is due to a maximum charge current of ~ 2 mA, which is limited by the current mirrors in our current design, and the fact that we tested our circuit on a relatively large and readily available 25 mAh lithium-ion battery. A 2 mAh battery, which is adequate for low-power applications, would have a charging time of approximately an hour. Larger-size current mirrors can decrease this charging time further but an excessively short charging time is usually deleterious to battery operation.

Our battery-management chip was fabricated in an AMI 0.5 μm CMOS process and consumes 0.15 mm² of chip area as shown in Fig. 19. We obtained a charging voltage accuracy of 99.8% relative to the target 4.2 V and power efficiency approximately equal to 75%, which is comparable to previous designs.

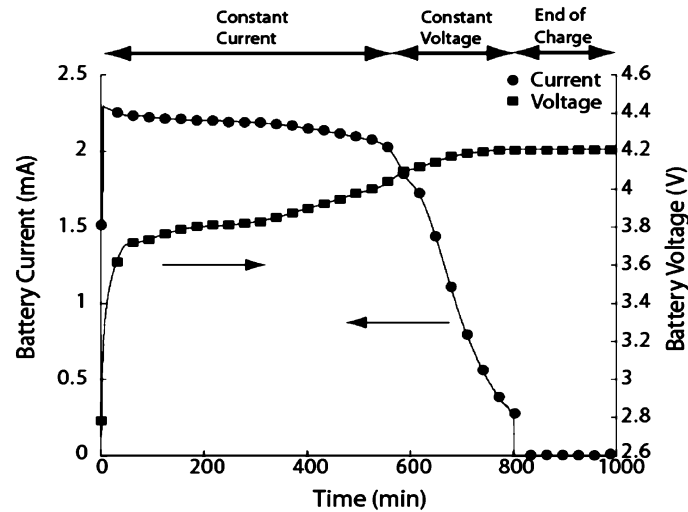


Fig. 18. Measured battery current and voltage when charging a 25 mAh battery with a ~ 2 mA maximum battery-charging current.

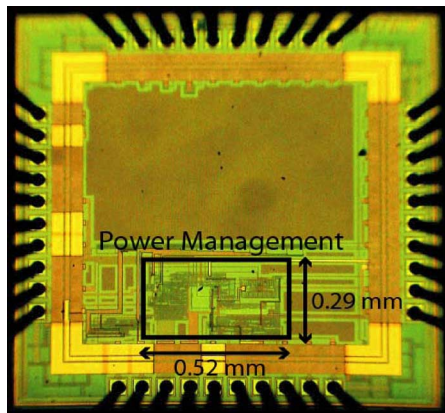


Fig. 19. Power-management die micrograph. The circuit measures 0.29 mm by 0.52 mm.

TABLE I
LI-ION BATTERY CHARGER DESIGNS COMPARISON

Design	Power Efficiency	Layout Area
[21]	67.9%	1.96 mm ²
[22]	82%	2.6 mm ²
[23]	83%	PCB
[24]	72.3%	Not Specified
This Work	75%	0.15 mm²

However, the layout area required for this chip is about an order of magnitude smaller than that of previous designs as shown in Table I.

In general, the size of the Li-ion battery required in any given application will scale proportionately with the needed load power consumption and inversely with the power density of the Li-ion battery [5]. The size of the current mirror in our charging circuit that is needed to recharge this battery in a fixed time will therefore scale with battery size or with load power. Wirelessly powered systems such as the inductive systems described in [20], or the antenna-based systems described in [6] and [25], must then be composed of RF power sources that can supply a power commensurate with their rectifier efficiency and with the desired battery recharging time.

VII. CONCLUSION

Ultralow-power cardiac-monitoring devices are a convenient and low-cost way to continuously monitor the cardiovascular system and to gather important clinical data. They are also a critical component of low-cost home-based tele-monitoring services. In this paper, we have presented integrated circuits for power reduction in such cardiac-monitoring devices. In particular, we have described three new ultralow-power sensor circuits: an electrocardiograph, a pulse oximeter, and a phonocardiograph. In addition, we have described a simple integrated-circuit switched-capacitor model of the heart. Finally, we have described a novel, ultracompact lithium-ion battery charging circuit intended for operation in a wirelessly rechargeable medical device.

REFERENCES

- [1] P. M. Rothwell, "Limitations of the usual blood-pressure hypothesis and importance of variability, instability, and episodic hypertension," *The Lancet*, vol. 375, no. 9718, pp. 938–948, Mar. 13, 2010.
- [2] Y. Ostchega, S. S. Yoon, J. Hughes, and T. Louis, Hypertension awareness, treatment, and control—Continued disparities in adults: United States, 2005–2006 National Center for Health Statistics, Hyattsville, MD, NCHS Data Brief no. 3, 2008 [Online]. Available: <http://www.cdc.gov/nchs/data/databriefs/db03.pdf>
- [3] Task Force Eur. Soc. Cardiol., North Amer. Soc. Pacing Electrophysiol., "Heart rate variability—Standards of measurement, physiological interpretation, and clinical use," *Circulation*, vol. 93, pp. 1043–1065, 1996.
- [4] Philips Med. Syst. North Amer. Corp., "TEN-HMS study demonstrates clinical and financial efficacy of home telemonitoring," Sep. 2003 [Online]. Available: http://www.alexianbrothershealth.org/pdf/tele-health_program.pdf
- [5] R. Sarpeshkar, *Ultra Low Power Bioelectronics: Fundamentals, Biomedical Applications, and Bio-inspired Systems*. Cambridge, U.K.: Cambridge Univ. Press, Feb. 2010.
- [6] L. Turicchia, S. Mandal, M. Tavakoli, L. Fay, V. Misra, J. Bohorquez, W. Sanchez, and R. Sarpeshkar, "Ultra-low-power electronics for non-invasive medical monitoring," in *Proc. Custom Integr. Circuits Conf. (CICC)*, Sep. 13–16, 2009, pp. 85–92.
- [7] R. Winter and J. Webster, "Reduction of interference due to common mode voltage in bio-potential amplifiers," *IEEE Trans. Biomed. Eng.*, vol. BME-30, pp. 58–62, 1983.
- [8] L. Fay, V. Misra, and R. Sarpeshkar, "A micropower electrocardiogram amplifier," *IEEE Trans. Biomed. Circuits Syst.*, vol. 3, no. 5, pp. 312–320, Oct. 2009.

- [9] M. Burke and D. Gleeson, "A micropower dry-electrode ECG preamplifier," *IEEE Trans. Biomed. Eng.*, vol. 47, no. 2, pp. 155–162, Feb. 2000.
- [10] T. Delbruck and C. Mead, "Adaptive photoreceptor with wide dynamic range," in *Proc. IEEE Int. Symp. Circuits Syst. (ISCAS)*, Jun. 1994, vol. 4, pp. 339–342.
- [11] P. Gray, P. Hurst, S. Lewis, and R. Meyer, *Analysis and Design of Analog Integrated Circuits*. Hoboken, NJ: Wiley, 2001.
- [12] M. Tavakoli, L. Turicchia, and R. Sarpeshkar, "An ultra-low-power pulse oximeter implemented with an energy-efficient transimpedance amplifier," *IEEE Trans. Biomed. Circuits Syst.*, vol. 4, no. 1, pp. 27–38, Feb. 2010.
- [13] S. Mandal, L. Turicchia, and R. Sarpeshkar, "A low-power battery-free tag for body sensor networks," *Pervasive Comput.*, vol. 9, no. 1, pp. 71–77, Jan.–Mar. 2010.
- [14] T. A. Parlikar, "Modeling and monitoring of cardiovascular dynamics for patients in critical care," Ph.D. dissertation, Dept. Electr. Eng., Mass. Inst. Technol., Cambridge, MA, 2007.
- [15] J. C. Bramwell and A. V. Hill, "The velocity of the pulse wave in man," *Proc. R. Soc. Lond. B*, vol. 93, no. 652, pp. 298–306, Apr. 1922.
- [16] P. Shaltis, A. Reisner, and H. Asada, "Calibration of the photoplethysmogram to arterial blood pressure: Capabilities and limitations for continuous pressure monitoring," in *Proc. IEEE Eng. Med. Biol. 27th Annu. Conf. (IEEE-EMBS)*, Shanghai, China, Sep. 1–4, 2005, pp. 3970–3973.
- [17] J. Bohorquez, W. Sanchez, L. Turicchia, and R. Sarpeshkar, "An integrated-circuit switched-capacitor model and implementation of the heart," in *Proc. First Int. Symp. Appl. Sci. Biomed. Commun. Technol. (ISABEL)*, Aalborg, Denmark, Oct. 25–28, 2008, pp. 1–5.
- [18] D. Linden and T. B. Reddy, *Handbook of Batteries*. New York: McGraw Hill, 2002, ch. 35.
- [19] S. Dearborn, "Charging Li-ion batteries for maximum run times," *Power Electron. Technol. Mag.*, pp. 40–49, Apr. 2005.
- [20] M. W. Baker and R. Sarpeshkar, "Feedback analysis and design of RF power links for low-power bionic systems," *IEEE Trans. Biomed. Circuits Syst.*, vol. 1, no. 1, pp. 28–38, Apr. 2007.
- [21] Y. S. Hwang, S. C. Wang, F. C. Yang, and J. J. Chen, "New compact CMOS Li-ion battery charger using charge-pump technique for portable applications," *IEEE Trans. Circuits Syst. I, Reg. Papers*, vol. 54, no. 4, pp. 705–712, Apr. 2007.
- [22] F. C. Yang, C. C. Chen, J. J. Chen, Y. S. Hwang, and W. T. Lee, "Hysteresis-current-controlled buck converter suitable for Li-ion battery charger," in *Proc. IEEE Int. Conf. Commun., Circuits Syst. (ICCCAS)*, Guilin, China, Jun. 2006, pp. 2723–2726.
- [23] M. Chen and G. A. Rincon-Mora, "Accurate, compact, and power-efficient Li-ion battery charger circuit," *IEEE Trans. Circuits Syst. II, Exp. Briefs*, vol. 53, no. 11, pp. 1180–1184, Nov. 2006.
- [24] C. C. Tsai, C. Y. Lin, Y. S. Hwang, W. T. Lee, and T. Y. Lee, "A multi-mode LDO-based Li-ion battery charger in 0.35 μm CMOS technology," in *IEEE Asia-Pacific Conf. Circuits Syst.*, Taiwan, Dec. 2004, pp. 49–52.
- [25] S. Mandal and R. Sarpeshkar, "Low-power CMOS rectifier design for RFID applications," *IEEE Trans. Circuits Syst. I, Reg. Papers*, vol. 54, no. 6, pp. 1177–1188, Jun. 2007.



Lorenzo Turicchia received the Laurea degree in electrical engineering from the University of Padova, Italy, and the Ph.D. degree in computer science from the Department of Mathematics and Computer Science, University of Udine, Italy.

He is a Research Scientist in the Research Laboratory of Electronics at the Massachusetts Institute of Technology (MIT), Cambridge. In 2002 he joined the Analog VLSI and Biological Systems group at MIT, where he completed his doctoral research. His main research interests are in nonlinear signal processing, especially for audio and biomedical applications, and bioelectronics. His work has included research on cochlear implants for the hearing impaired, visual prostheses for the blind, speech prostheses for individuals with severe communication disabilities, automatic speech recognition in noise, and wearable medical devices. In these areas he has authored 7 patent applications and more than 40 publications. He is currently working on robust techniques for the recognition of speech, speaker, and language in noisy environments; bioelectronics for wearable and implantable medical devices; and neural decoding techniques for neural prosthetic devices for the paralyzed.



Bruno Do Valle (S'03) received the B.S. (*summa cum laude*) and M.S. degrees in electrical engineering from Boston University, Boston, MA, in 2006 and 2008, respectively. He is currently working toward the Ph.D. degree at Massachusetts Institute of Technology (MIT), Cambridge, in the Analog VLSI and Biological Systems Group at the MIT Research Laboratory of Electronics.

His research interests include low-power analog and mixed-signal VLSI for biomedical applications, and power electronics for low-power applications.



Jose L. Bohorquez (S'04–M'09) received the B.S. and M.S. degrees in electrical engineering from the University of Florida, Gainesville, in 2002 and 2004, respectively, and the Ph.D. degree from the Massachusetts Institute of Technology, Cambridge, in 2009, where his research focused on ultralow-power circuits and systems for medical implants.

He held internships at APA Wireless, Lockheed Martin, and GE Healthcare, and in 2004 joined Bit-Wave Semiconductor where he designed analog and RF blocks for a reconfigurable transceiver. He is currently

President and CEO of Convergence Medical Devices, Inc., Winchester, MA, a startup company that he cofounded.

Dr. Bohorquez has received several awards, including the International Engineering Consortium's William L. Everitt Student Award of Excellence, the Semiconductor Research Corporation/IBM Fellowship, and the MIT Presidential Fellowship.



William R. Sanchez received the B.S. degree in electrical engineering and computer science and the M.Eng. degree in electrical engineering and computer science from the Massachusetts Institute of Technology (MIT), Cambridge, in 2005 and 2007, respectively. He is currently working toward the Ph.D. degree in the Microsystems Technology Laboratory at MIT.

He is engaged in research in the design of energy-efficient, ultralow-power circuits and systems for wireless biomedical communications and applications. His current research interests include power electronics, waste heat recovery and energy harvesting, and small antenna design.



Vinith Misra received the B.S. and M.Eng. degrees in electrical engineering from the Massachusetts Institute of Technology, Cambridge, in 2008. He is currently working toward the Ph.D. degree in electrical engineering from Stanford University, Stanford, CA.

His research interests include information theory, signal processing, and mixed-signal circuits, with an emphasis on the intersection between theory and practice.



Leon Fay received the B.Sc. and M.Sc. degrees in electrical engineering from the Massachusetts Institute of Technology, Cambridge, in 2008.

Currently, he is a Research Engineer with SRI International, Menlo Park, CA, in the communications, radar, and sensors group. He is working on low-power wireless sensors for harsh environments, signal-processing techniques for radar image reconstruction, and algorithms for high-speed tracking with impulse radar.



Maziar Tavakoli received the B.Sc. degree in electrical engineering from Sharif University of Technology, Tehran, Iran, in 1998 and the M.Sc. and Ph.D. degrees in electrical engineering from the Massachusetts Institute of Technology (MIT), Cambridge, in 2001 and 2005, respectively, where he worked on developing high-performance electronics for MEMS vibration sensors and pulse oximeters, respectively.

His research interests included analog VLSI circuit design for biomedical and sensory systems. He is now working at Linear Technology Corporation, North Chelmsford, MA.



Rahul Sarpeshkar (M'98–SM'07) received B.S. degrees in electrical engineering and physics from the Massachusetts Institute of Technology (MIT), Cambridge, and the Ph.D. degree from the California Institute of Technology, Pasadena.

He was with Bell Labs as a Member of Technical Staff in the Department of Biological Computation within its Physics Division. Since 1999, he has been on the faculty of MIT's Electrical Engineering and Computer Science Department, where he heads a research group on Analog VLSI and Biological Systems. He authored the recent text *Ultra Low Power Bioelectronics: Fundamentals, Biomedical Applications and Bio-inspired Systems*, which provides a broad and deep treatment of the fields of low-power electronics and bioelectronics. He holds over 25 patents and has authored more than 100 publications, including one featured on the cover of *Nature*.

Dr. Sarpeshkar has received several awards, including the NSF Career Award, the ONR Young Investigator Award, the Packard Fellows Award, and the Indus Technovator Award for his interdisciplinary bioengineering research. He is an Associate Editor of the IEEE TRANSACTIONS ON BIOMEDICAL CIRCUITS AND SYSTEMS and serves on the program committees of several technical conferences.